Functionalization of a chemically treated Ti6Al4V-ELI alloy with nisin for antibacterial purposes

Applied Surface Science 620 (2023) 156820

Contents lists available at ScienceDirect

Applied Surface Science

journal homepage: www.elsevier.com/locate/apsusc

Full Length Article

# Functionalization of a chemically treated Ti6Al4V-ELI alloy with nisin for antibacterial purposes

Virginia Alessandra Gobbo [a,*], Mari Lallukka [b], Francesca Gamna [b], Mirko Prato [c], Alessandra Vitale [b], Sara Ferraris [b], Ziba Najmi [d], Andrea Cochis [d], Lia Rimondini [d], Jonathan Massera [a], Silvia Spriano [b]

[a] Faculty of Medicine and Health Technology, Tampere University, 33720 Tampere, Finland
[b] Department of Applied Science and Technology, Politecnico di Torino, 10129 Torino, Italy
[c] Materials Characterization Facility, Istituto Italiano di Tecnologia, Via Morego 30, 16163 Genova, Italy
[d] Department of Health Sciences, Center for Translational Research on Autoimmune and Allergic Diseases – CAAD, Università Del Piemonte Orientale UPO, Corso Trieste 15/A, 28100 Novara, Italy

ARTICLE INFO

*Keywords:*
Titanium alloy
Surface modification
Protein adsorption
Antimicrobial peptides
Nisin
Antibacterial properties

ABSTRACT

This research aims to define a protocol for nisin adsorption onto Ti6Al4V- Extra Low Interstitial content (ELI) alloy to reduce the risk of *peri*-implant infections. The substrate is, first, etched to get a nanotextured surface with a high density of acidic hydroxyl groups and then functionalized with the antimicrobial peptide nisin. Nisin adsorption is performed at different pH values, in the range of 5–7. The nisin release in inorganic solutions mimicking physiological or pro-inflammatory conditions is tested. The surfaces are characterized by profilometry, SEM/EDS, contact angle and surface free energy measurements, zeta potential titrations, DLS, XPS, and UV–visible spectroscopy. Effective surface adsorption was achieved and maximized at pH 6. The coated surface has high surface energy suitable for tissue integration and it releases nisin in a time longer than 1 day. As a confirmation of the antibacterial properties due to the nisin adsorption, specimens were incubated with *Staphylococcus aureus*, whose metabolic activity was reduced by ≈ 70% in comparison to the untreated control, and the number of viable adhered colonies was ≈ 6 times reduced. In conclusion, coupling of nisin to a chemically treated titanium surface is promising for a bioactive and antibacterial surface for tissue integration.

## 1. Introduction

Titanium and its alloys are optimal materials for orthopedic and dental applications because of high biocompatibility, low toxicity, high fatigue strength, and relatively low Young's modulus as requested for bone implants [1,2]. Nevertheless, titanium surfaces can be improved with other interesting properties. Bioactivity and fast osseointegration can be induced by either physical and/or chemical surface treatments. Osteoconductive and osteoinductive surfaces can be imparted through micro- and/or nano-roughness or tailored porosity, without altering the bulk properties of titanium. Chemical and physical surface modification can be induced by exploiting a wide range of techniques (etching, sandblasting, plasma treatment, photolithography, laser or e-beam texturing, freeze-casting), while plasma spray, electrochemical deposition, and sol–gel coatings are the main applied techniques for surface coating [3–9]. The etched surface used in this research has a proven positive biological response and bioactive behavior [6,10].

Due to the evidence that bacterial infections are nowadays a major reason for implant failure, it is requested to provide a significant antibacterial (active) and/or antimicrofouling (passive) activity on biosurfaces for bone contact [6,10]. Antibacterial properties have become of particular interest because of the increasing resistance that bacteria are showing against antibiotics in the last years. The data collected by the World Health Organization (WHO) in 2018 and 2019 demonstrate how the rate of resistance of common bacteria, such as *Escherichia coli*, *Klebsiella pneumoniae* and *Staphylococcus aureus*, reached respectively 92.9%, 79.4%, and 64.0% against the drug treatments routinely applied in clinics (ciprofloxacin and methicillin) prior and after surgery [11]. This problem, mainly ascribable to the abuse and misuse of antibiotics, is leading to the increasing difficulty to fight bacterial infections. As a consequence, it is rapidly increasing the risk of local and systemic infections after surgical operations and during hospitalization, which may

* Corresponding author.
*E-mail address:* virginiaalessandra.gobbo@tuni.fi (V. Alessandra Gobbo).

https://doi.org/10.1016/j.apsusc.2023.156820
Received 16 November 2022; Received in revised form 27 January 2023; Accepted 18 February 2023
Available online 24 February 2023

cause the failure of the implant and its consequent removal, with serious effects on the health of the patients [12]. Different strategies have been tested in this context and different approaches can be implemented at the same time to further increase the effectiveness of the antimicrobial systems exploitable for implantable materials [13,14].

A first strategy consists of anti-adhesiveness (antimicrofouling): surfaces are treated to prevent bacteria adhesion, thus inhibiting the subsequent stratification that brings the drug-resistant 3D biofilm conformation. In this view, it is possible to apply super-hydrophobic surfaces, so that the anti-adhesion activity is implemented by the surface's physical and chemical properties [13,15,16]. Unfortunately, these surfaces are usually not suitable for osseointegration. It is also possible to get a nanostructured topography, through e-beam surface treatments for example, able to discourage bacteria adhesion due to the impossibility to adapt their cytoskeleton to the irregular surface nanotopography [17,18].

The second approach consists instead of a bactericidal strategy: bacteria can adhere to the surface, but their membrane is degraded by pre-adsorbed antibacterial compounds, leading to the disruption of bacteria themselves (anti-biofilm or anti-proliferation strategies). In this way, the development of biofilm is strongly limited, so the risk of infection is significantly reduced. It is possible to adsorb, graft, or encapsulate either ions, pre-designed nanoparticles, or even biomolecules with intrinsic antimicrobial/bactericidal properties: in proper concentrations, they have a targeted toxic behavior against bacteria, but not against human cells. Among this class of biomolecules, antimicrobial peptides (AMPs) have raised interest due to their high variety, their ability to be grafted to various types of surfaces by exploiting different mechanisms, and their wide antibacterial spectrum against both Gram-negative and Gram-positive bacteria [14].

One of the most promising AMPs for designing antimicrobial surfaces is nisin, already approved by the Food and Drug Administration (FDA) and applied in the food industry as a natural food preservative pertaining to its highly effective antibacterial properties and, at the same time, its safety and biocompatibility [19]. Nisin is naturally produced by bacteria appertaining to *Lactococcus, Streptococcus,* and *Staphylococcus* species and it is classified as a class I bacteriocin, also referred to as a lantibiotic. The chemical structure of nisin consists of a series of 34 amino acids (AAs) and it is characterized by the presence of multiple S-bridges connecting some AAs to obtain polycyclic structures among the molecule [19–21]. This molecule has a relatively low molecular mass (lower than 5 kDa, generally ranging from 1.8 to 4.6 kDa), it is amphiphilic, and it has a net positive charge (+4) at physiological pH [19–22]. Its antimicrobial activity is effective within a wide range of temperatures (until around 100 °C, with an optimal stability around 25 °C in acidic conditions) against a wide range of bacteria, mainly the Gram-positive ones, and certain types of viruses and fungi [19–23]. The biological activity of nisin covers also immunomodulatory properties [19].

Because of the discussed properties of nisin, recently it has started to be studied as a grafted or adsorbed biomolecule on the surface of biomaterials to limit bacteria adhesion, to induce bacteria death, also disrupting eventual dangerous mutated cells [20], and, consequently, to decrease the risk of infections and post-surgical complications. Various techniques are currently studied – such as direct grafting, physical adsorption, and covalent bonding through coupling agents – to graft an adequate amount of biomolecule in a biologically active configuration [24–27].

The authors have previously investigated nisin physisorption on the polished titanium alloy Ti6Al4V with Extra Low Interstitial content (Ti64ELI) in [28], as it was considered an interesting substrate for musculoskeletal application. The low content of interstitials (0.12 wt% of oxygen content against 0.20 wt% characterizing the more common Ti6Al4V) increases toughness, resistance to corrosion, and crack propagation [29]. Nisin was physisorbed on the polished substrate and exercised an activity of inhibition of the formation of bacteria microcolonies (biofilm-like aggregates) [28]. However, because of inert surface, no bioactivity was observed inducing any osteoconductive effect. Furthermore, a limited amount of nisin was detected on the coated surface, due to the low surface area and to the non-specific interactions between the peptide and the material.

In the present study, the substrate was treated with a patented chemical treatment [30] to obtain a surface able to induce apatite precipitation (bioactive), suitable for osseointegration, and with antimicrofouling properties (low adhesion of bacteria) [6,31]. The grafting of nisin to this specific substrate allows the combination of osteogenic and antibacterial properties on the same surface optimized for bone contact permanent implants. Nisin direct grafting was introduced on this substrate, exploiting its topography, high surface-to-volume ratio, and the presence of a high density of functional groups (–OH) to increase the amount of the linked peptide, with the intent to enrich the surface with active antibacterial properties. A direct grafting procedure was selected to avoid the use of any toxic linker. Finally, the ability of the nisin-grafted surfaces to reduce the infection of the *Staphylococcus aureus* pathogen was verified in comparison to the untreated controls.

## 2. Materials and Methods

### 2.1. Samples preparation

The considered substrate was Ti6Al4V with Extra Low Interstitial content (Ti64ELI, provided by Titanium Consulting and Trading, Firenze, Italy). The samples were 10 mm-diameter and 2 mm-thick discs, obtained by transversally cutting a bar through a lathe. They were successively polished with a series of SiC papers from 320 to 4000 grit (P320, P500, P800, P1200, P2400, P4000) to obtain a surface with controlled roughness. The polished Ti64ELI samples are referred to as Mechanically Polished (MP). MP samples were sonicated once in 50 ml of acetone for 5 min and then twice in 50 ml of ultra-pure water for 10 min, to remove any possible impurity, and dried under a laminar hood. The chemical treatment was then applied, as previously described [6,30], following a patented protocol which consists of an acid etching with hydrofluoric acid (HF) to remove the native oxide, followed by controlled oxidation in hydrogen peroxide ($H_2O_2$). The goal of this treatment is the formation of a micro- and nanotextured titanium oxide layer, rich in –OH groups [6]. The so-obtained samples are referred to as Chemically Treated (CT).

### 2.2. Surface activation

To optimize the nisin adsorption, the surface of CT samples was activated through a 1-hour treatment by UV irradiation (UV-C 40 W, 253.7 nm) [32]. This process was applied to remove eventual contaminations from the atmosphere and adsorbed water molecules, and, in the meanwhile, to promote the exposition of the –OH groups enhancing the reactivity of the surface itself.

### 2.3. Nisin adsorption

Nisin A (Nisin Ready Made Solution; 20,000–40,000 IU/mL in 0.02 N HCl, Sigma Aldrich) was diluted into ultra-pure water to obtain a solution with the final concentration of 1 mg/ml [24,33]. Three different pH conditions (pH 5, pH 6, and pH 7) were then imposed for nisin adsorption. The nisin solution (pH = 3.39 ± 0.05) was so buffered by adding dropwise 0.05 M NaOH buffer solution and, if needed, 0.05 M HCl, until the target pH value was reached. These three pH conditions were selected with the rationale to avoid any risk of corrosion of the substrate and to maximize the electrostatic attraction between the molecule and the substrate (as explained in the Results section), and were compared to optimize the adsorption process finding the most efficient condition for adsorbing this polypeptide.

The three aforementioned pH values were selected, as successively discussed in paragraph 3.3.1, as the conditions for which the charge

difference between CT and the nisin solution was maximized. The adsorption was then implemented in the pH range 5–7, where the nisin, as confirmed by literature, still maintains its antimicrobial properties [23]. The original pH of nisin solution was not considered because soaking titanium in such acidic condition would lead to a strong corrosion [34,35]. This could cause an uncontrolled variation in the surface morphology and a significant damage to the textured oxide layer obtained by previous etching.

Each CT sample, after having been UV-activated, was then placed into a 24-well plate; 1 ml of the diluted nisin solution, at the imposed pH condition, was added to completely cover the surface and the samples were incubated for 24 h at room temperature. After this time, each sample was removed, rinsed in ultra-pure water, and dried under the laminar hood. The samples with adsorbed nisin at the three pH conditions are referred to as CT Nisin5, CT Nisin6, and CT Nisin7, respectively.

To have a reference, three control CT samples were parallelly prepared, UV-activated, and soaked in ultra-pure water previously buffered at the three pH conditions (pH 5, pH 6, pH 7), following the protocol for nisin adsorption, but without any nisin addition into the solution. The control samples are referred to as CT ctrl5, CT ctrl6, and CT ctrl7, respectively.

The three as-prepared nisin solutions (pH 5, pH 6, pH 7) and all the uptake solutions (either with nisin, for the adsorption, or without nisin, for the control), from which the CT samples were extracted after soaking, were then analyzed by measuring their pH through a pHmeter (Edge pH, HANNA Instruments). All the measurements were made in triplicate.

### 2.4. Physical-chemical characterization

#### 2.4.1. Contact profiler and confocal microscopy

To quantify the surface roughness of samples, a contact profiler (Talysurf Intra Touch, Taylor Hobson) and a confocal laser scanning microscope (LSM 900, Zeiss) were utilized. Both MP and CT were analyzed to be compared. With the contact profiler, (5x5) $mm^2$ areas were acquired, while, through the confocal microscope, the considered areas were (250x250) $\mu m^2$. The experiment was made in triplicate. The data acquired through both instruments were successively processed with the same protocol. Utilizing the AnalysisTool software, the images were un-tilted and filtered by applying in series a high-pass filter with a cut-off wavelength of 8 μm for the waviness, and a low-pass filter with a cut-off wavelength of 250 μm for the roughness. The parameters of interest, the superficial roughness (Sa), root mean square height (Sq), skewness (Ssk), and kurtosis (Sku), expressed in nm, were eventually extracted according to the normative DIN EN ISO 4287 and DIN EN ISO 4288.

#### 2.4.2. Field emission scanning electron microscopy – Energy dispersive spectroscopy (FESEM/EDS)

FESEM/EDS (FESEM - SUPRATM 40, Zeiss) was used to observe the surface of both MP and CT samples. The images were acquired at two different magnifications, respectively 60kx and 150kx. The electron high tension (EHT) voltage was set at 10 kV. The observations were made in triplicate. The EDS analysis was carried on to quantify the amount (expressed as an atomic percentage, atomic %) of titanium (Ti), aluminum (Al), vanadium (V) and oxygen (O). The electron high tension (EHT) voltage was set at 15 kV for the EDS analysis. Three areas per each image were randomly selected and the atomic content of the elements of interest was measured.

#### 2.4.3. UV–Vis spectroscopy

An UV-spectrophotometer (UV2600 Shimadzu) was utilized to analyze both nisin solutions and solid samples. Concerning liquid samples, the measurements were carried out to evaluate the absorbance spectrum of each considered solution within the wavelength range of 190–750 nm. Concerning solid samples, the reflectance spectrum in the same range was recorded through an integration tool (ISR-2600Plus, a two-detector integrating sphere). All the measurements were made in triplicate.

#### 2.4.4. Contact angle analysis and surface free energy calculation

Static contact angle measurements were performed by means of a FTA 1000C instrument, equipped with a video camera and image analyzer, at room temperature. Three probe liquids were used: ultra-pure water, hexadecane, and ethylene glycol (all from Sigma Aldrich, St. Louis, USA), whose surface tension is 72.1 mN/m, 28.1 mN/m, and 48.8 mN/m, respectively. Three measurements were performed on each sample, placing the liquid drops in different parts of the sample surface: the mean value and the error were determined. The overall surface energy, as well as its polar and dispersive components, were calculated by the Owens-Wendt geometric mean method [36] using the contact angle values measured with water and hexadecane.

#### 2.4.5. Zeta potential and dynamic light scattering (DLS) analysis

Zeta potential analysis was performed on both nisin solutions and solid samples.

Concerning solid samples, zeta potential titration curves were acquired by an electrokinetic analyzer (SurPASS 2, Anton Paar). Using the adjustable gap cell for discs, two samples of the same type were parallelly placed at a distance of about 100 μm, inserted into the instrument, and the zeta potential was measured as a function of pH, while the electrolyte (1 mM KCl solution), buffered by an automatic titration unit utilizing 0.05 M HCl and 0.05 M NaOH solutions, was flowing between them. Two different couples of samples were used for respectively evaluating the acidic and the basic range, properly rinsing the instrument between the two measurements, after having placed the new couple of samples. The titration started at pH 5.5 for both the pH ranges and the automatic titration unit added the buffer solutions for each of the total 15 buffering steps (the explored pH range is between pH 2.5 to 10). For each pH value, three zeta potential values were measured and averaged.

Concerning liquid samples, the nisin solution was analyzed by acquiring a zeta potential titration curve by an electrophoretic analyzer (Nanosizer Nano Z, Malvern Instrument, Malvern). Nisin was dissolved in the electrolyte (1 mM KCl) to obtain a 1 mg/ml solution (corresponding to the concentration utilized for adsorption on CT samples). The electrolyte was then buffered with 0.05 M HCl and 0.05 M NaOH solutions, respectively, to totally have 8 solutions in the pH range 3–9. Through the same measurement, the hydrodynamic radius was also measured.

The isoelectric point (IEP) was finally extracted as the intersection between the titration curve and the abscissa axis or calculated by interpolation.

#### 2.4.6. X-ray photoelectron spectroscopy (XPS)

XPS analysis (XPS, Kratos, Axis Ultra$^{DLD}$ spectrometer) was performed on reference (MP, CT, CT ctrl5, CT ctrl6, CT ctrl7) and coated samples (CT Nisin5, CT Nisin6, and CT Nisin7). On each surface, 3 different areas (300x700 $\mu m^2$ each) were stochastically selected and, for each of them, both the survey scan (0–1200 eV) and high-resolution spectra on selected elements (Ti 2p, O 1 s, C 1 s, N 1 s, S 2p) were acquired, respectively at pass energy of 160 eV (energy step = 1 eV) and pass energy of 20 eV (energy step = 0.1 eV). All the analyses were run using a monochromatic Al Kα source ($h\nu$ = 1486.7 eV), operated at 20 mA and 15 kV. To compensate for the charging effect, the Kratos charge neutralizer system was utilized. The reference of all the spectra was implemented setting the hydrocarbon C 1 s peak at 284.80 eV. Spectra were processed by CasaXPS software (version 2.3.24) [37].

#### 2.4.7. Release tests

To evaluate the stability of the nisin adsorbed on CT Nisin6, a release

test in function of time was assessed. CT Nisin6 was selected as the most efficiently coated surface, according to the zeta potential analysis, for the optimized properties, as more deeply explained in paragraph 3.3.1. The eventual release of the polypeptide was studied by soaking the material of interest for 7 days. Two solutions were considered: phosphate-buffered saline (PBS tablet, Sigma-Aldrich), for mimicking a physiological condition, and an acidic solution containing hydrogen peroxide (referred to as $H_2O_2$), for simulating a pro-inflammatory condition. Hydrogen peroxide (30% w/v, PanReac Applichem) was added to PBS to reach a concentration of 0.05 M and then buffered with HCl to pH 4.5 [38]. Each sample of interest (CT Nisin6) was immersed in 5 ml of the respective solution and, parallelly, control samples (CT ctrl6) were soaked in the same conditions, as a reference. At the end of the soaking, the samples were gently washed in ultra-pure water. The wettability of the surfaces was evaluated after 1 day and 7 days by contact angle analysis utilizing the sessile drop method (Kruss DSA 100). A 5 µl drop of ultra-pure water was gently placed on the surface of interest, the software associated with the instrument (Drop Shape Analysis) automatically recorded the left and the right angles and the average was given in the output.

#### 2.4.8. Antibacterial properties evaluation

*2.4.8.1. Strain growth condition.* Bacteria were purchased from the American Type Culture Collection (ATCC, Manassas, USA). Specimens' antibacterial properties were assayed towards the methicillin/oxacillin (MRSA) resistant *Staphylococcus aureus* strain (Gram-positive, ATCC 43300). Bacteria were cultivated in Trypticase Soy agar plates (TSA, Sigma-Aldrich) and incubated at 37 °C until round single colonies were formed; then, 2–3 colonies were collected and spotted into 15 ml of Luria Bertani broth (LB, Sigma-Aldrich) and incubated overnight at 37 °C under agitation (120 rpm). The day after a fresh broth culture was prepared before the experiments by diluting bacteria into a fresh medium to a final concentration of $1 \times 10^3$ bacteria/ml, corresponding to an optical density of 0.00001 at 600 nm wavelength using a spectrophotometer [39] (Spark, from Tecan, Switzerland).

*2.4.8.2. Bacterial metabolism, number, and morphology evaluation.* The International Standard ISO 22196 was applied to evaluate specimens' antibacterial properties [40]. Accordingly, the specimens (CT Nisin6, CT Nisin3 and non-functionalized CT – CT ctrl, considered as control) were located into a 24-multiwell plate; then, 50 µl of the bacterial suspension adjusted at a final concentration of $1 \times 10^3$ bacteria was directly dropped onto the specimens' surfaces. To compare the antimicrobial properties of nisin when adsorbed on the substrates at pH = 6 with the activity of nisin at the original pH conditions, the samples prepared with the pH = 3 nisin stock solution were also evaluated for their ability in preventing bacterial colonization.

The inoculated specimens were placed in an incubator at 37 °C for 24 h. Afterward, the colorimetric Alamar blue assay (AlamarBlue™, Life Technologies) was applied to test viable bacteria metabolic activity by spectrophotometry following the manufacturer's instructions. Briefly, the ready-to-use Alamar solution at concentration 0.0015% in PBS was added to each well containing the test specimen (1 ml per specimen), and the plate was incubated in the dark for 4 h at 37 °C allowing resazurin dye reduction into fluorescent resorufin upon entering living cells. Then, 100 µl were spotted into a black-bottom 96-well plate to minimize the background signal. The metabolic activity of bacteria was measured via spectrophotometer ($\lambda_{ex} = 570$ nm and $\lambda_{em} = 590$ nm), and the results were presented as Relative Fluorescent Units (RFU).

Then, to investigate the number of viable bacteria adhered on the samples' surface the Colony Forming Unit (CFU) count was performed. Briefly, after washing 2 times with PBS to remove non-attached bacterial cells, the samples were submerged into 1 ml of PBS, sonicated and vortexed for 5 min and 30 s, respectively (three times). Next, an aliquot of 200 µl of the bacteria suspension was collected and transferred to a new 96 wells plate; here, 6 serials 1:10 dilutions were performed by mixing progressively 20 µl of the bacterial suspension with 180 µl of PBS. Then, 20 µl of each serial dilution were spotted into a LB agar plate and incubated for 24 h until round colonies were visually checked; the final number of CFU was calculated by using the following formula [41]:

CFU = [ (number of colonies × dilution factor) (serial dilution) ].

Finally, Scanning Electron Microscopy (SEM, JSM-IT500, JEOL) imaging was used to investigate the morphology of bacteria grown onto specimens' surfaces; briefly, specimens were dehydrated by the alcohol scale (70–90-100% ethanol, 1 h each), swelled with hexamethyldisilazane, mounted onto stubs with conductive carbon tape and covered with a gold layer. Images were collected at different magnifications (2000X and 5000X) using secondary electrons.

### 2.5. Statistical analysis of data

Experiments were performed in triplicate. Results were statistically analyzed using the SPSS software (v.20.0, IBM, USA). Groups were compared by the one-way ANOVA using the Tukey's test as a post-hoc analysis. Significant differences were established at $p < 0.05$.

## 3. Results

### 3.1. Physical-chemical characterization of the MP and CT samples

#### 3.1.1. Profilometer and confocal microscopy

Roughness and topography of CT and MP were measured both with a contact profiler and a confocal laser scanning microscope (Fig. 1). Both techniques confirmed a significant increase in roughness of the substrate after the chemical treatment. The topographical parameters are reported in Table 1.

The optical way of measurement of the confocal microscope is more accurate at the nanoscale than the contact one, that characterizes the contact profiler, which is instead accurate at the microscale. Because of this, the two techniques can be considered complementary, since they highlight different features. The increase in surface roughness characterizing the CT samples, registered both by the profilometer and confocal microscope (Sa values, Table 1), can be attributed to the micro- and nanostructuring induced by etching, confirming the successful surface treatment [6]. The CT surface has a lower roughness than the average of commercial implants, but it has been proven that it is beneficial for the biological response and a lower roughness is preferred in terms of high fatigue resistance and low biofilm formation [6,42].

After the chemical treatment, the surface also shows a higher root mean square (Sq) deviation. The Sq/Sa ratio on MP and CT is respectively 1.3 and 1.4 Considering that a reference value of 1.25 refers to a Gaussian shape of the surface features, a sharper shape is expected for the investigated samples, as the Sq/Sa value is higher. Sku values are always higher than 3, confirming an overall spiked distribution with a significant increase on CT, suggesting a more spiked distribution after etching. The obtained values are in line with what reported as optimal for the surface morphology of HF treated titanium surfaces for osseointegration even if the absolute value of roughness is lower [43]. Considering the Ssk values, the height distribution is skewed above the mean plane before etching (0.988) and it is the opposite on the treated sample (-1.18) according to the presence of porosity. All the investigated topographical parameters associated with CT agree with the presence of a porous oxide layer and nanometric dimples induced by etching [6]. The presence of this topography on the CT surface is of interest to enhance the physical entrapment of the polypeptide during the adsorption process.

#### 3.1.2. Field emission scanning electron microscopy – Energy dispersive spectroscopy (FESEM/EDS)

FESEM was performed on the CT samples to observe the micro- and

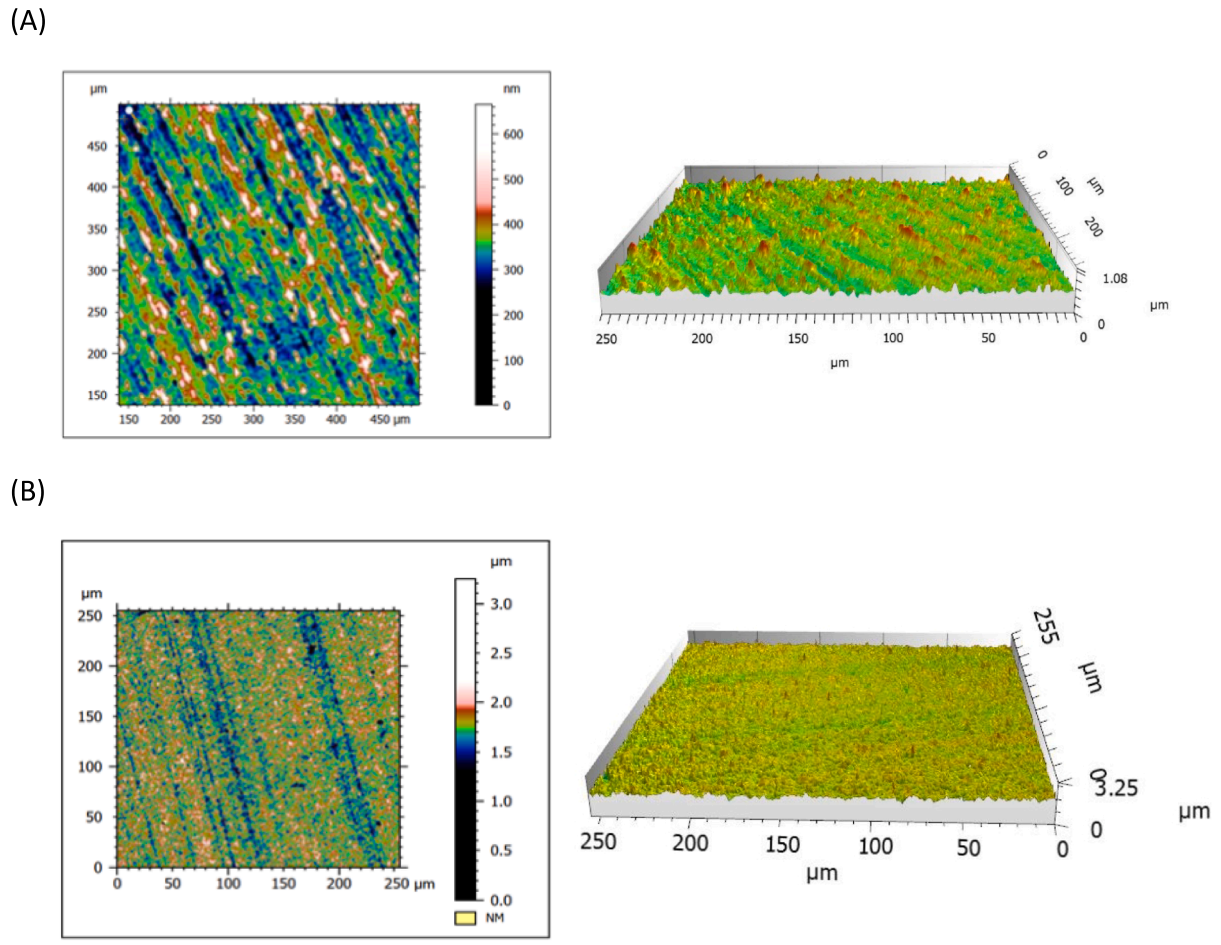


**Fig. 1.** Roughness and topography analysis by confocal microscope of the surface of (A) MP and (B) CT.

**Table 1**
Topographical parameters - Sa and Sq (expressed in nm) and Ssk and Sku values – of MP and CT evaluated through contact profiler and confocal microscope.

| SAMPLE | Ti64ELI | |
|---|---|---|
| | Contact profiler | Confocal microscopy |
| **Sa values (nm)** | | |
| **MP** | 39.6 | 38.4 |
| **CT** | 56.2 | 74.7 |
| **Sq values (nm)** | | |
| **MP** | 53.4 | 51.1 |
| **CT** | 73 | 104 |
| **Ssk values** | | |
| **MP** | – | 0.988 |
| **CT** | – | −1.18 |
| **Sku values** | | |
| **MP** | – | 5.1 |
| **CT** | – | 22.2 |

nanoscale morphology of the substrate. The MP samples were observed as control. In Fig. 2, the images of MP and CT surfaces obtained by FESEM are reported, at two different magnifications (60kx, 150kx).

While MP is characterized by a smooth surface, on which it is possible to see some irregularities due to mechanical polishing, a uniform micro- and nano-textured surface is clearly visible on the CT samples. The surface has a multiscale roughness which can contribute to a successful absorption of nisin. The roughness at the microscale (observed in Figure B.1 as smooth ridges and valleys of about 1 µm apart) is due to chemical etching in HF. A porosity with few nanometers-sized pores is due to oxidation in hydrogen peroxide and it covers the whole surface of the samples. These observations are in agreement with roughness analysis and it has been proven that a micro- and nano-roughness is beneficial for osseointegration [6].

Furthermore, the atomic percentage of the elements was analyzed before (MP) and after (CT) the chemical treatment, through EDS analysis. The results are reported in Fig. 3.

EDS shows a significant difference in the chemical composition of Ti64ELI after etching. The atomic percentage of titanium (Ti) is drastically reduced from 63% to 40%, while the content of oxygen (O) increases around twice (from 27% to 54%). This result highlights the higher thickness of the titanium oxide layer on CT, compared to the native one on MP, due to the chemical treatment. The characteristics of the obtained surface oxide layer on CT are the same as already published by the authors on a Ti6Al4V alloy grade 5 [6] in terms of chemistry, roughness, and topography. It means that even if Ti6Al4V ELI grade has a different corrosion resistance from grade 5, the surface properties of CT are analogue. Because of this, the authors assume that all the surface properties of Ti6Al4V ELI are the same as Ti6Al4V alloy grade 5, more deeply investigated by the authors in previous works [6]. The presence of a thicker (around 180 nm) and continuous oxide layer on the CT surface is here of interest to guarantee good corrosion resistance during the adsorption process and implantation life, as well as to enhance the grafting ability of the polypeptide [6].

### 3.2. *Characterization of the nisin solutions*

The nisin solutions (1 mg/ml) were analyzed by UV–Vis spectroscopy before performing nisin adsorption on CT samples. In Fig. 4(A), the absorbance spectra of the nisin solutions at different pH values are

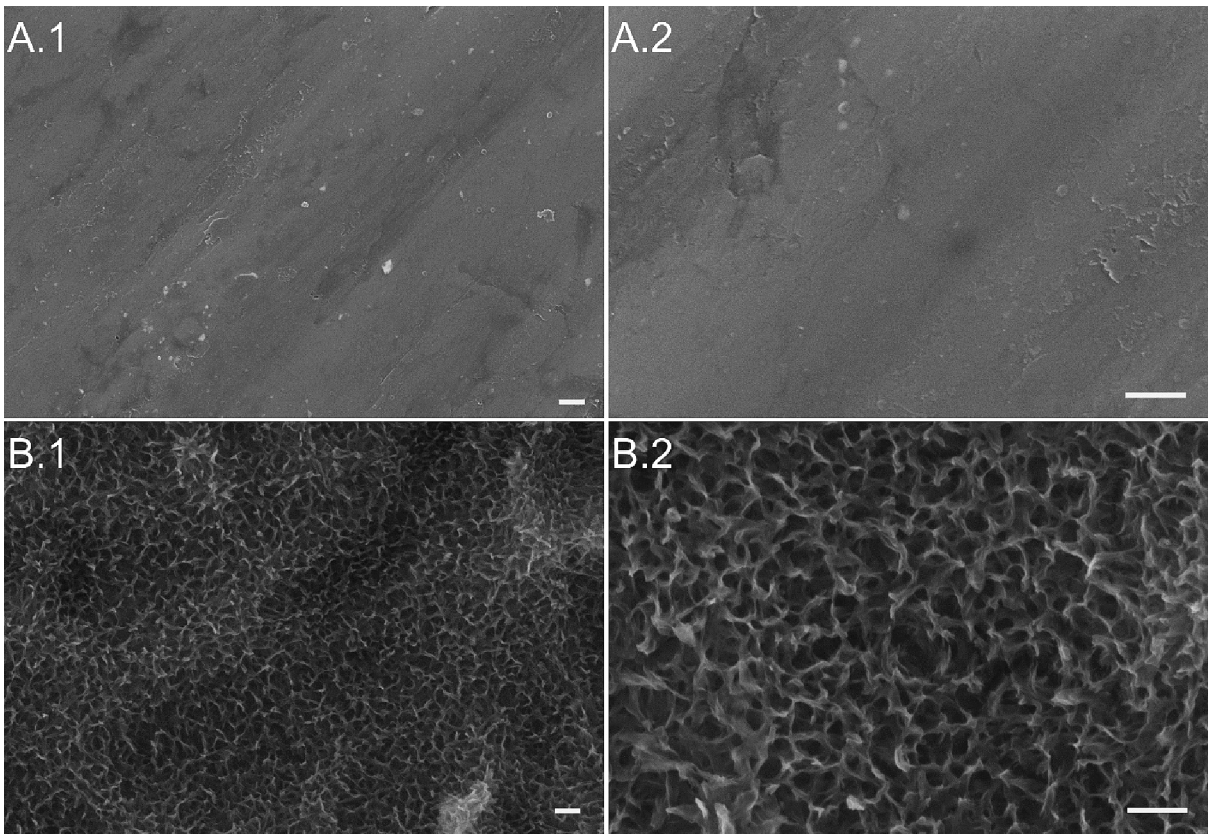


**Fig. 2.** FESEM images of the surface of the MP samples with (A.1) magnification 60kx, (A.2) magnification 150kx, and of the surface of the CT samples with (B.1) magnification 60kx, (B.2) magnification 150kx. The scalebar corresponds to 200 nm on all the panels.

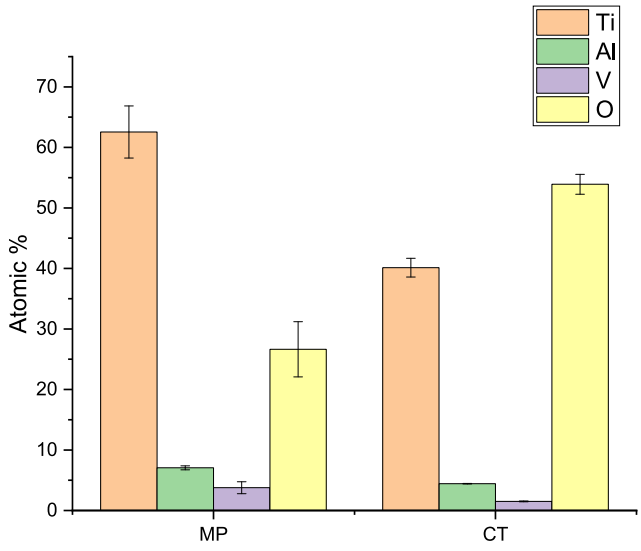


**Fig. 3.** EDS analysis of Ti64ELI samples before (MP) and after (CT) the chemical treatment. The chemical composition is expressed as atomic percentage (Atomic %).

reported (the original pH of the stock solution and the three imposed values pH 5, pH 6, and pH 7). In accordance with the literature, the main peak is observed at 250 nm in the aqueous solutions at the imposed pH values in the range of 5–7. This peak can be ascribed to free nisin, confirming the proper dissolution of the polypeptide in these solutions [44,45]. A shoulder superimposed to the main peak is detectable at around 270–280 nm and can be attributed to the spontaneous formation of some small nisin nanoparticles [45]. All the solutions show a comparable absorbance value at 270–280 nm; the solution at pH 5 has a slightly lower intensity that is not significant. No red or blue shift of the peak at 270–280 nm is evident confirming that in these solutions the dimension of the nanoparticles is comparable.

The aqueous nisin solution (1 mg/ml) was characterized by a zeta potential titration curve (Fig. 4(B)), investigating its zeta potential for a wide range of pH values (from 3 to 9) in a KCl solution diluted to 1 mM (low ionic strength). The isoelectric point (IEP) was detected at 7.5, dividing the curve into two main branches. At alkaline pH (higher than 7.5) the negative charge of AAs is prevalent, mainly due to the deprotonation of carboxylic groups. In the acidic range, AAs has a net positive charge. The absolute value of zeta potential is not higher than 12 mV for both the basic and acidic range, which means that the nisin net charge in the investigated condition is not strong. A low net charge value of nisin is also reported in [46]. From a theoretical calculation, the IEP of nisin is expected to be 8.8 [47]; the difference can be explained considering the low absolute value of the registered zeta potential and high sensitivity of zeta potential to the ionic strength of the solution.

Through the DLS measurements (Fig. 4(C)), the hydrodynamic diameter of nisin in aqueous solutions (1 mg/ml) at different pH was also measured. The hydrodynamic diameter is about 400–600 nm at pH between 3 and 7, while it grows up to 1.2 μm above pH 8, indicating that the colloidal suspension becomes less soluble, as expected, around the IEP. Low solubility is maintained above the IEP probably because degradation of nisin occurs in an alkaline environment [48].

According to the results obtained from the zeta potential titration curve, it was decided to perform the adsorption processes at pH 5, 6, and 7. In this range nisin has an overall positive charge, with an increasing amount of deprotonated carboxylic groups and zwitterionic form moving towards pH 7. Any alkaline pH was excluded since, according to the measured hydrodynamic diameter of nisin in aqueous media, the

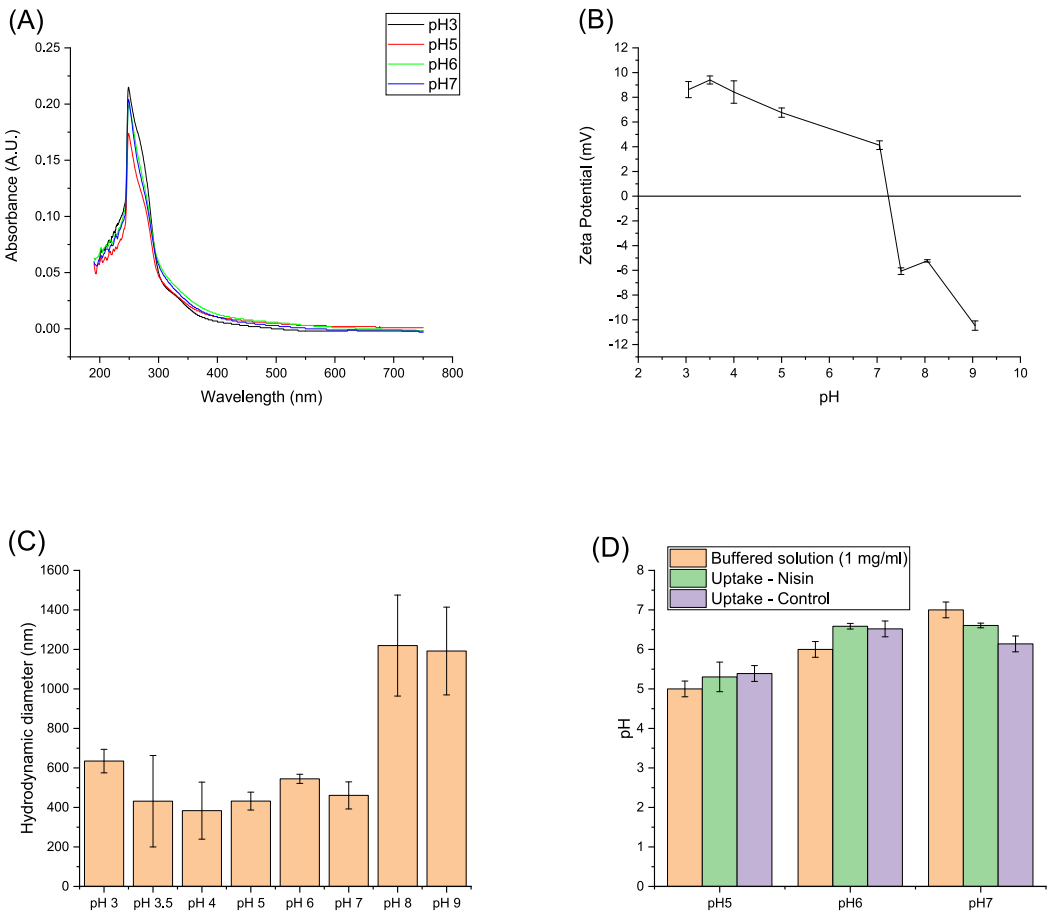


**Fig. 4.** Characterization of 1 mg/ml nisin solutions by (A) UV–Vis spectroscopy, (B) zeta potential analysis, and (C) hydrodynamic diameter of nisin, measured by DLS analysis, in aqueous solution (1 mM KCl) as a function of pH. (D) pH values of the buffered nisin solutions, nisin uptake solutions, and control uptake solutions (CT soaked in buffered solutions without nisin) at pH5, pH6, and pH7, respectively.

colloidal suspension becomes unstable; no pH value below 5 was used to avoid corrosion of the metal substrate.

The pH value of the nisin solutions has been measured before and after having soaked the CT samples (Fig. 4(D)). The pH values of the control uptake solutions, in which the CT samples were soaked in a buffered solution without nisin (as described in paragraph 2.3), are also reported as a reference. Analyzing the histogram, it is possible to appreciate that the differences are small and ascribable to environmental reasons (such as $CO_2$ dissolution), rather than to any significant change occurring during the adsorption process, considering that the

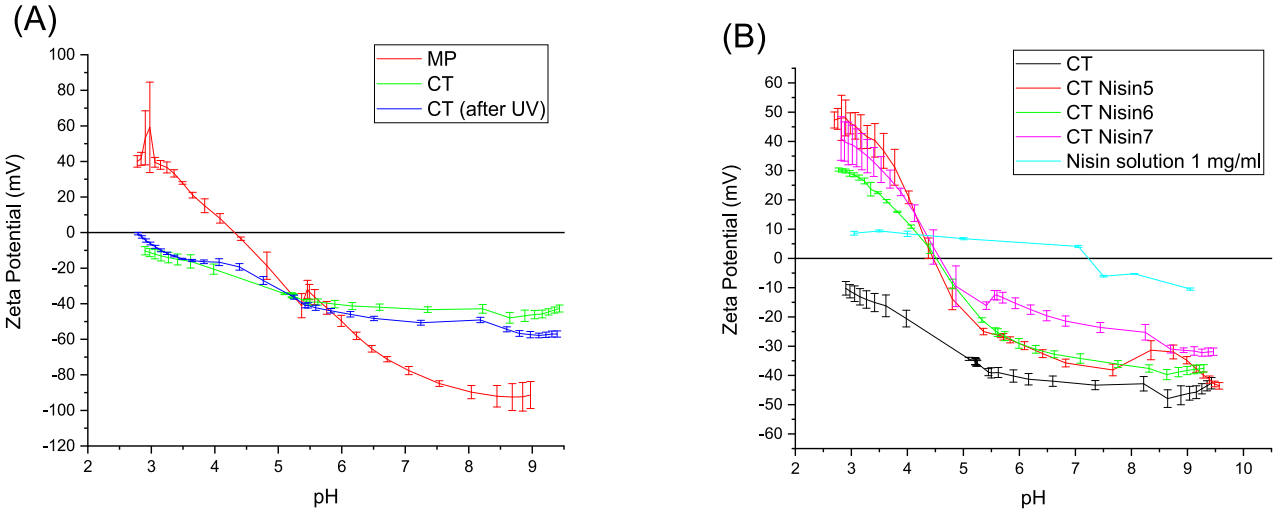


**Fig. 5.** (A) Zeta potential titration curves of Ti64ELI before (MP) and after (CT) the chemical treatment and of CT after UV activation. (B) Zeta potential titration curves of Ti64ELI before (CT) and after (CT Nisin5, CT Nisin6, CT Nisin7) nisin adsorption; the zeta potential titration curve characterizing the nisin solution (1 mg/ml) is also reported.

controls follow the same trend as the uptake solutions.

### 3.3. Characterization of the nisin-coated samples

#### 3.3.1. Zeta potential analysis

The surface zeta potential was measured on the CT samples both before and after UV activation and compared to MP as a control (Fig. 5 (A)). In Fig. 5(B), the zeta potential titration curves of CT before and after nisin adsorption are reported. In Table 2, the IEP values of each surface of interest and nisin solution are shown.

The effects of the chemical treatment on the surface are evident by observing the shape and IEPs of the titration curves. The IEP detected on the MP samples (pH = 4.4) is in accordance with literature for the standard titanium alloy Ti6Al4V: it is the typical value of a surface with almost no functional groups with a strong acid-basic reactivity [49,50]. The chemical treatment induces a shift of the IEP down to 2.2 on the CT samples, attributable to the presence of functional groups with a strong acidic behavior. The CT samples are also chemically stable in a wide range of pH, as appreciable by the low standard deviation characterizing each point of zeta potential and as expected because of the formation of a thicker oxide layer: this is of relevance considering that pH can change from 7.4 down to 4.5 *in vivo* at the inflammatory conditions [51]. The absence of corrosion phenomena is also important during the process of functionalization.

The CT curve is characterized by a lower slope of the curve around the IEP than the MP one, which is related to higher hydrophilicity: the water molecules are strongly adsorbed on the CT surface and not easily replaced by the ions in solution (hydroniums or hydroxyls) by changing pH. The CT curve stabilizes in a plateau around −45 mV at pH 5–6 and remain almost constant in the whole basic region. All the described phenomena (IEP shift, high hydrophilicity, and the plateau in the alkaline range) can be explained by the exposition on the surface of a high amount of hydroxyl groups with strong acidic behavior, which are progressively deprotonated at pH 2–6 and completely deprotonated at higher pH [31,50]. These groups can be exploited for nisin grafting, as discussed in the following. Furthermore, the CT samples maintain the same behavior even after UV irradiation, excluding a slightly higher IEP due to the exposition of some hydroxyl groups with a basic chemical behavior. At the pH values selected for nisin adsorption, the CT substrate has a net negative surface charge and, at least, partially deprotonated –OH groups, while nisin has an overall positive charge. With these conditions, an electrostatic attraction can be predicted between the substrate and the biomolecule.

A significantly different shape of the titration curve and shift of IEP toward higher values is evident after nisin adsorption, compared to CT. The IEPs of the functionalized surfaces do not match that of nisin in solution: at this stage, this phenomenon can be ascribed to incomplete coverage of the surface.

CT Nisin5, CT Nisin6, and CT Nisin7 have all an intense positive charge on their surface in the strongly acidic range (zeta potential reaches values around 30 and 50 mV at pH 3, while the values for CT are around −15 and −10 mV), suggesting the successful adsorption of the polypeptide and the fully protonated state of the amino (and carboxylic) groups at low pH, as expected. In the alkaline range, the surface zeta potential of the coated samples is different (milder) than CT, ulteriorly confirming the presence of nisin adsorbed on the surface.

The different slope of the titration curve of the functionalized surfaces with respect to the polypeptide in an aqueous solution (Fig. 5(B)) can be ascribed to a higher hydrophobicity of the grafted polypeptide with respect to the native polypeptide in solution: the exposition of the hydrophilic moieties of the grafted polypeptide can be assumed to be towards the surface and the hydrophobic ones towards the solution. Looking at the primary structure of nisin, we can hypothesize that the un-polar and hydrophobic amino acids (like alanine, glycine, proline, valine, methionine, isoleucine, leucine), normally buried inside the polypeptide core, could be exposed outermost after the functionalization process. The opposite could occur for the polar (serine, asparagine) and charged (lysine, histidine) amino acids, which are expected to be attracted by the substrate surface [52].

Furthermore, it is possible to see some significant differences between the functionalized samples prepared at different pH values. CT Nisin6 samples show a different curve mainly in the acidic range: this difference can be due to a lower amount, or different orientation, of the grafted polypeptide with respect to the other samples. CT Nisin5 and CT Nisin7, instead, show a stronger and comparable zeta potential with no statistical difference in the acidic range. The curves of CT Nisin5 and CT Nisin7 are both characterized by an unstable behavior in this range, as the high standard deviations of zeta potential suggest, while CT Nisin6 has low standard deviations, and it is much more stable. This feature can be related to different stability of the bond between the surface and the grafted polypeptide. A less stable electrostatic interaction can be assumed in the case of the functionalization performed at pH5 and 7. An attempt of explanation is here reported. On one hand, the –OH groups on the CT surface are not completely deprotonated at pH 5 and, on the other hand, the zwitterionic form of the polypeptide is almost prevalent at pH 7 with a lower net charge of the molecule. In both cases, the electrostatic attraction between the substrate and biomolecule can be supposed to be weaker. Differently, the difference in the surface charge is expected to be maximized at pH 6 with a more stable grafting through electrostatic attraction. It is because of the maximized electrostatic interaction that CT Nisin6 was selected for further release and antibacterial analyses.

#### 3.3.2. X-ray photoelectron spectroscopy (XPS)

To compare the presence of nisin on the different surfaces and quantify the elements of interest on each surface, XPS analysis was performed on CT, CT ctrl5, CT ctrl6, CT ctrl7, CT Nisin5, CT Nisin6 and CT Nisin7. In Table 3, the composition of the considered surfaces is reported, and the high-resolution spectra of C, N, O, and S acquired on the functionalized samples CT Nisin5, CT Nisin6, and CT Nisin7 are compared to those acquired on CT in Fig. 6.

All the acquired spectra show the presence of Ti and O, the elements

**Table 2**
IEPs characterizing Ti64ELI before (MP) and after (CT) the chemical treatment, CT after UV activation and after nisin adsorption (CT Nisin5, CT Nisin6, CT Nisin7). IEP of nisin solution (1 mg/ml) is also reported.

| | IEP |
|---|---|
| MP | 4.4 |
| CT | 2.2 |
| CT (after UV) | 2.7 |
| CT Nisin5 | 4.5 |
| CT Nisin6 | 4.5 |
| CT Nisin7 | 4.6 |
| Nisin solution 1 mg/ml | 7.5 |

**Table 3**
Composition of the surface of each sample by XPS. The results are expressed as atomic percentages (at%).

| Sample | O (at %) | C (at %) | N (at %) | Ti (at %) | Al (at %) | S (at %) | Ca (at %) |
|---|---|---|---|---|---|---|---|
| **CT** | 53.1 | 20.7 | 2.0 | 21.6 | 2.6 | 0.0 | 0.0 |
| **CT ctrl5** | 42.8 | 38.7 | 1.3 | 14.3 | 2.8 | 0.0 | 0.0 |
| **CT ctrl6** | 54.8 | 18.6 | 2.1 | 21.9 | 2.5 | 0.0 | 0.0 |
| **CT ctrl7** | 51.9 | 22.9 | 1.3 | 19.9 | 2.9 | 0.0 | 1.1 |
| **CT Nisin5** | 32.4 | 49.9 | 7.8 | 8.4 | 0.9 | 0.4 | 0.3 |
| **CT Nisin6** | 33.5 | 46.5 | 8.4 | 9.7 | 1.0 | 0.8 | 0.2 |
| **CT Nisin7** | 30.5 | 51.0 | 7.3 | 8.2 | 1.3 | 0.9 | 0.7 |

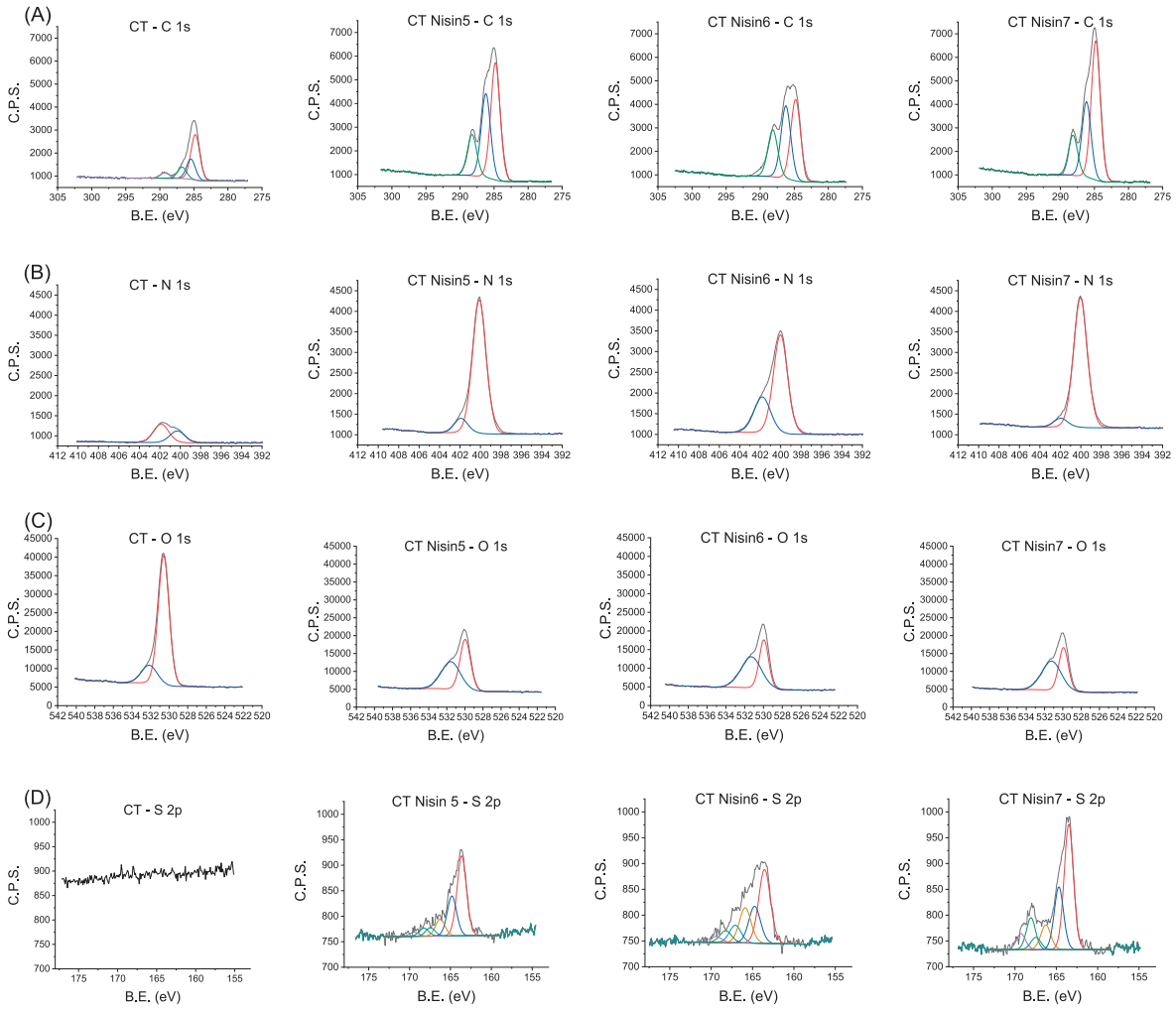


**Fig. 6.** High-resolution spectra of (A) C 1 s, (B) N 1 s, (C) O 1 s, and (D) S 2p acquired on CT, CT Nisin5, CT Nisin6, CT Nisin7 by XPS analysis. The binding energy (B. E.) is expressed in eV and the relative area in arbitrary units.

of the oxide layer characterizing the CT samples. C, N, and S, which are the elements of the nisin molecule, have a significant increase on the functionalized samples (CT Nisin5, CT Nisin6, CT Nisin7), confirming the presence of the polypeptide on the functionalized samples. C and N are also present in the spectra of the control samples (CT, CT ctrl5, CT ctrl6, and CT ctrl7 – not reported), nevertheless with a significantly lower intensity with respect to the functionalized samples, assigned to adventitious impurity adsorbed from the atmosphere or solutions, always present onto titanium surfaces [53,54]. The fact that the signal attributed to Ti is still detectable after nisin adsorption could be explained either by a partial surface coverage or by a homogeneous, but very thin nisin layer, with a thickness below 5–10 nm [55].

The successful adsorption of nisin is also appreciable by the significant modifications of the high-resolution spectra acquired on the surfaces before (CT) and after nisin adsorption at the three considered pH conditions (CT Nisin5, CT Nisin6, CT Nisin7). After nisin adsorption (Fig. 6(A)), an intense C 1 s peak at (286.2 ± 0.2) eV appears, which is attributed to the presence of C-O/C-N and C = O bonds [25]. Furthermore, the presence of the component at (288.2 ± 0.2) eV, characteristic of carbon in peptide bonds (O=C-N), ulteriorly confirms the presence of nisin on the surface and the effective adsorption which cannot be confused with other adventitious organic contaminants [26,27].

The overall content of nitrogen (Fig. 6(B)) increases after nisin adsorption, as indicated by the increased intensity of N 1 s peaks at (400.1 ± 0.2) eV and (401.9 ± 0.2) eV, attributed to neutral amine $NH_2$ and protonated amine $NH_3^+$ groups, respectively [56]. The relative amount of $NH_3^+$ groups is higher in the CT Nisin6 sample, revealing a specific type of bonding of the polypeptide, at this pH, through the charged amino groups. The presence of the positively charged functional groups is of interest because nisin exercises its antimicrobial activity by electrostatically interacting through these groups with the cell wall precursor lipid II, which is bound to the cytoplasmatic membrane of the target bacteria. This interaction alters the equilibrium of the membrane of the bacterium and induces the formation of pores, which leads to the death of the micro-organism [21].

The presence of the adsorbed layer on the nisin-coated samples as a non-covering layer is confirmed by the profile fitting of the oxygen region (Fig. 6(C)). The peak due to the Ti-O bond of the titanium oxide layer, always observable at (530.1 ± 0.4) eV, has a lower intensity on all coated samples, as expected. The peak at (531. 6 ± 0.4) eV can be attributed both to the –OH functional group of CT and also to the peptidic bond in the case of the coated samples.

Concerning S 2p (Fig. 6(D)), this element is not detectable on CT, while the spectra acquired after nisin adsorption can be interpreted assuming the presence of three different sulphur states. Each S chemical state is fitted with a doublet of peaks, separated by 1.2 eV and with a ratio of 2:1 between the so-called 3/2 (component at lower binding energy) and 1/2 (component at higher binding energy) components. The main one, with S $2p_{3/2}$ centered at (163.6 ± 0.2) eV, is attributed to the thiol -SH groups which are present in the molecular structure of AAs

constituting nisin [26]. The others are characterized by S $2p_{3/2}$ centered at (166.1 ± 0.2) eV and (168.2 ± 0.2) eV; both are symptomatic of oxidation of the thiol groups to sulphonyl and sulphonate groups, respectively [57].

As last, the presence of calcium ions on the functionalized surfaces is in line with previous observations [31] and suggests that it has a role in the functionalization mechanism as a linker between the negatively charged functional groups of CT and nisin. This is different from what observed after functionalization with nisin of mechanical polished Ti6Al4V-ELI where the substrate has not such a high density of deprotonated functional groups and physisorption instead of chemisorption occurred [28].

### 3.3.3. Surface free energy calculation

Surface free energy was calculated on the surface of Ti64ELI before (MP) and after (CT) the chemical treatment, and after nisin adsorption at pH6 (CT Nisin6). For this characterization, the surface coated with nisin at pH6 was selected according to the previous results. The values of the total surface energy (γ), together with its dispersive $\gamma^d$ and polar $\gamma^p$ components, are reported in Table 4.

Comparing MP and CT, it is clear that the chemical treatment is inducing an increase in the total surface free energy of the substrate, which is mainly due to the higher polar component characterizing CT, while the dispersive component remains constant. This is in accordance with the zeta potential analysis, which highlighted the presence of hydroxyl groups on the CT surface, the main cause of a more hydrophilic surface and, consequently, a higher polar component. After nisin adsorption, no significant difference was detected, since comparable values of γ, $\gamma^p$, and $\gamma^d$ are observed on the substrate both before (CT) and after (CT Nisin6) nisin adsorption. This is of relevance because a threshold of 40 mN/m is reported as a general rule for cell adhesion on surfaces and tissue integration: hydrophobic surfaces with lower surface energy are usually cytotoxic, while hydrophilic surfaces with higher surface energy are usually suitable for tissue integration, and surfaces with surface energy just at the threshold value are nor cytotoxic neither adhesive for the cells (e.g. osteoblasts) [58,59].

CT substrate both before (CT) and after (CT Nisin6) nisin adsorption has proven to show a super-hydrophilic behavior (contact angle with water of (4.5 ± 0.9)° and (7.1 ± 1.6)° for CT and CT Nisin6, respectively). Interestingly, the same behavior was observed also towards organic solvents (e.g., hexadecane and ethylene glycol), characterized by different polarities and surface tensions. The contact angles of CT and CT Nisin6 are in fact (3.7 ± 0.4)° and (4.6 ± 0.3)° for hexadecane, (4.2 ± 0.7)° and (5.4 ± 0.5)° for ethylene glycol, respectively. This is of relevance considering that the simulated and real physiological fluids have lower surface tension than water (as low as 55 mN/m) and that good wettability by physiological liquids is required for tissue integration [60]. In conclusion, the nisin-coated surface here developed can be supposed to be suitable for integration with the biological tissues.

### 3.3.4. Characterization after the release tests

The eventual release of nisin from the coated surfaces during soaking in two solutions, respectively mimicking the physiological and pro-inflammatory conditions, was tested. A surface nisin-coated at pH6 has been selected according to the previous results. The eventual presence of nisin on the surface after the release tests was tested through contact angle analysis. The results are reported in Table 5. Control samples (with no nisin adsorption) soaked in the same conditions have been also tested as a reference.

As a general trend, the soaking in both the solutions induces a higher wettability on all surfaces with a decrease of the contact angle after soaking. The nisin-coated samples shows a lower decrease of the contact angle with respect to the control after soaking for 1 day in both the solutions evidencing that nisin is still present on the surface, at this time point. The control and coated surfaces acquire a similar (reduction of 63% vs 100%) or identical (contact angle 0°) wettability after 7 days of soaking in PBS or $H_2O_2$. It can be assumed that the release is almost complete at this stage. This behavior is significantly different from that of polished and functionalized Ti6Al4V-ELI alloy as reported in [28] where the change in contact angle after the release test, compared to the functionalized surface, was lower in all cases. It can be concluded that the CT surface is able to release a larger amount of grafted nisin than the polished one; a role of physisorption instead of chemisorption in the different release can be supposed. The release of nisin is of relevance for fighting the risk of infection that is higher in the first days after surgery [20]. According to these data, a double mechanism of action can be expected from the functionalized surface in a biological environment: a release in the surrounding liquids that can counteract the floating planktonic bacteria, and direct inhibitory contact with the biofilm bacteria trying to adhere and colonize the surface of the device [20]. This is of great interest considering that AMPs hold a double activity, direct and indirect, towards bacteria. AMPs grafted on the surface can directly bind to the negatively charged membrane phospholipids causing bacteria death due to irreversible pores formation, as well as by the inhibition of the ATPase activity, thus preventing chaperone-assisted protein folding [61,62]. In parallel, AMPs released in the physiological fluids can promote the recruitment of neutrophils at the infection site, thus activating the immunological cascade thus indirectly counteracting the infection [62,63]. In the specific case of nisin, even if its concentration is lower than the minimum inhibitory concentration (MIC), this molecule can still regulate the toxic activity of bacteria by downregulating the expression of the toxin-encoding genes [63–65].

### 3.3.5. Antibacterial properties evaluation

According to the previous physicochemical characterization, the CT Nisin6 specimens were selected for the antibacterial evaluation due to their superior ability in terms of nisin adsorption in comparison to the CT Nisin5 and CT Nisin7, besides the non-functionalized CT control (CT ctrl). Etched CT specimens were selected as control over the bulk MP ones due to their roughness depending by the nanotexture as previously shown by the SEM images (Fig. 2 B1-B2); in fact, such texture confer anti-adhesive properties due to the presence of the nanopeaks preventing bacteria anchorage in the early adhesion phase [17]. So, to precisely evaluate the contribution of the nisin per se the CT specimens have been used to rank the results of the nisin-doped ones.

Moreover, considering that the bioactivity of nisin is known to be pH-dependent, specimens obtained by using the pH3 nisin stock solution from the manufacturer (here named as CT Nisin3) were exploited and

**Table 4**
Surface energy γ, and its dispersive $\gamma^d$ and polar $\gamma^p$ components, of the surface of chemically treated Ti64ELI before (CT) and after nisin adsorption (CT Nisin6). MP is reported as a control.

| | Surface energy (mN/m) | | |
|---|---|---|---|
| | γ | $\gamma^d$ | $\gamma^p$ |
| MP | 55.7 ± 1.3 | 27.4 ± 0.1 | 28.3 ± 1.3 |
| CT | 73.0 ± 0.1 | 27.4 ± 0.0 | 45.6 ± 0.1 |
| CT Nisin6 | 72.7 ± 0.3 | 27.4 ± 0.0 | 45.3 ± 0.3 |

**Table 5**
Percentage change of contact angle (water) on the surfaces of CT Nisin6 and CT ctrl6 (as reference) after 1 day and 7 days of soaking in PBS and a solution mimicking the inflammatory condition (called $H_2O_2$).

| | Change of contact angle vs d0 | |
|---|---|---|
| **PBS** | **CT Nisin6** | **CT ctrl6** |
| d1 | −27% | −100% |
| d7 | −63% | −100% |
| **$H_2O_2$** | **CT Nisin6** | **CT ctrl6** |
| d1 | −47% | −100% |
| d7 | −100% | −100% |

compared to the CT Nisin6 specimens' results to confirm that the grafted nisin did not reduce its bioactivity due to the pH variation as we previously demonstrated by comparing MP and MP nisin-doped specimens where the latter showed a promising antifouling activity by preventing the formation of 3D biofilm-like structures [28].

As prior detailed in the Materials and Methods section, the pathogen *Staphylococcus aureus* was used to directly infect the surface of the materials. *S. aureus* was selected because it is frequently involved in bone infections after clinical revisions, as well as the inoculum concentration ($1x10^3$ bacteria) was applied as it is reported by literature being the minimum number of bacteria potentially leading to septic condition after surgery [66].

The results are reported in Fig. 7. According to bacterial metabolic activity (Fig. 7(B)) detected after 24 h of direct contact with the specimens' surfaces, the viability of bacteria adhered to the CT Nisin6 significantly decreased up to 80% (±11%, ≈6-folds reduction) in comparison with non-functionalized CT controls (Fig. 7(B), $p < 0.05$ indicated by the §); moreover, the CT Nisin6 resulted as significant towards the CT Nisin3 specimens too (Fig. 7(B), $p < 0.05$ indicated by the #), thus confirming the surface absorption of bioactive nisin at pH6 as previously suggested by the physical–chemical characterization.

The metabolic evaluation was then confirmed by the CFU count (Fig. 7(A); in fact, a significant reduction of the number of viable colonies (between 1 and 1.5 logs) colonizing specimens' surface was detected by comparing CT Nisin6 with the CT controls (Fig. 7(A), $p < 0.05$ indicated by the §) and the CT Nisin3 as well (Fig. 7(A), $p < 0.05$ indicated by the #); therefore, it can be hypothesized that the reduction of the metabolic activity detected onto the specimens' surface is due to the significant reduction of the viable colonies adhered onto the CT Nisin6 specimens. Therefore, the antibacterial effect of the nisin grafted onto the CT surface resulted as much more evident in comparison to the MP specimens where only an inhibition of 3D colonies and biofilm formation was observed whereas the CFU number resulted as not significantly decreased in respect to the untreated controls [28]. Such improvement can be probably ascribed to the higher affinity of the nisin towards the negative charged CT surface as well as to a synergistic effect of the nanotexture preventing adhesion and nisin counteracting proliferation and biofilm formation.

Finally, as further confirmation of the nisin bioactivity, SEM images were collected to check the colonization degree of the specimens as well as the morphology of the bacteria (Fig. 7(C)). In line with previous results, the surface of the CT Nisin6 specimens showed the lower degree of contamination in comparison to the CT control and CT Nisin6. Moreover, higher magnification images revealed that bacteria adhering to the CT Nisin6 surfaces were mostly growing as single colonies whereas in the CT control and CT Nisin3 some 3D biofilm-like aggregates were found, thus suggesting for anti-microfouling activity due to the nisin higher bioactivity onto the CT Nisin6 specimens as previously observed for the MP specimens, too [28].

Summarizing these results, it can be hypothesized that the chemical treatment applied to the Ti surface was successful in increasing or stabilizing the nisin adsorption probably due to the negatively charged nanotextured layer and a chemisorption mechanism. Moreover, the obtained results are in line with previous literature. Najmi et al. (2020) compared the antibacterial activity of nisin at physiological pH against two Gram-positive bacteria, *Staphylococcus aureus* and *Staphylococcus epidermidis*, and two Gram-negative bacteria, *Escherichia coli* and *Aggregatibacter actinomycetemcomitans*. Based on their results, nisin is more effective toward Gram-positive bacterial strains than Gram-negative ones [62].

Regarding the nisin anti-microfouling activity few literature is available but the presence of nisin was previously shown by Blackman et al. [67] to reduce the surface contamination from bacterial aggregates in combination with a specific patterning as well as Kim et al. [68] demonstrated that the presence of nisin conferred outstanding fouling resistance to ultrafiltration PDMA membranes when infected.

As it was previously reported, in Gram-negative bacteria, because of the presence of the outer membrane, the nisin binding to the cellular

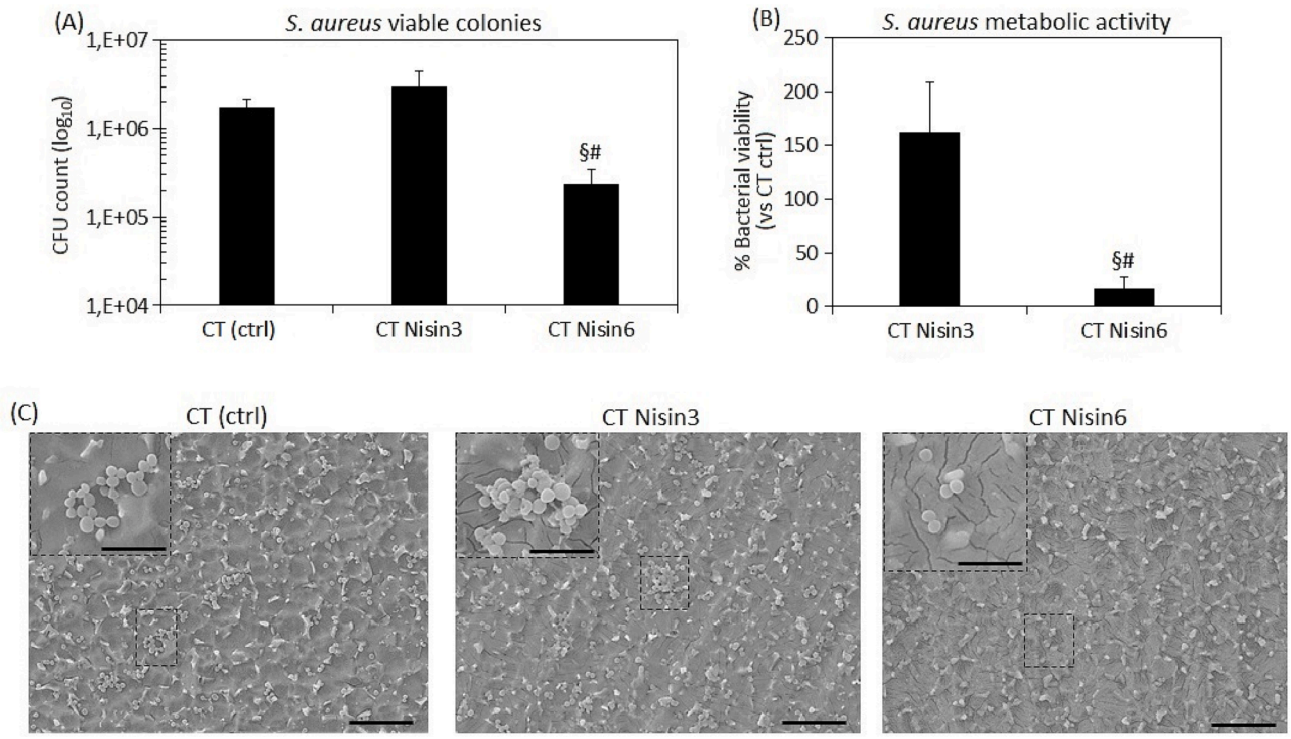


**Fig. 7.** Antibacterial activity of Ti-functionalized with nisin at pH3 and pH6. A) Metabolic activity of bacterial cells normalized towards non-functionalized CT (ctrl); B) Viable bacterial colonies count (CFU). C) SEM images at two magnifications: 2000X (scalebar = 10 mm) and 5000X (scalebar = 5 mm). § and # indicates $p < 0.05$. Replicates n = 3.

membrane (Lipid II) is complicated. Roupie et al. (2021) created nisin-based layer-by-layer coatings on glass coverslips to simultaneously prevent bacterial attachment and foster osseointegration. After preparation of glass coverslips with different layers, they were submerged into nisin Z solution for 24 and 48 h; their results revealed that nisin Z immobilization increased its antibacterial activity in comparison with free nisin and based on contact time, after 48 h a reduction of 92.5% in bacterial attachment observed [69].

Accordingly, the here presented results confirmed that nisin can be considered an interesting and suitable natural molecule conferring antibacterial properties to biomaterials, even if it should be considered that it is more effective towards Gram-positive pathogens. CT shows to be a substrate suitable for an effective functionalization with nisin: it allows chemisorption of nisin and effective release of the molecule. This was not the case for the mechanically polished Ti6Al4V-ELI as shown in [28]. As last, the mild anti-microfouling action of CT [17] can be useful to inhibit eventual bacterial adhesion at long time after implantation when the release of nisin is completed and no more effective.

## 4. Conclusions

An effective surface functionalization with nisin can be performed on a chemically treated titanium alloy surface avoiding the use of any toxic linker, by exploiting the surface topography, with nanometric dimples, and surface chemistry, with a high density of acidic hydroxyl groups. The adsorption of the polypeptide can be performed in the pH range within 5 and 7 and it is maximized at pH 6, where the difference in the electrostatic attraction between the surface (with deprotonated hydroxyl groups) and the polypeptide (with a prevalence of the positively charged form) is the highest. The higher surface area, compared to the untreated substrate, and the more specific chemical interaction with the peptide allows to obtain an effective chemisorption. The nisin-coated surface has a high surface energy and wettability suitable for tissue integration, further enhanced by the bioactivity of the chemically treated substrate itself. Moreover, it releases nisin, with a not complete release after 1 day both in physiological and inflammatory simulated conditions, and almost total after 7 days. The mild antimicrofouling action of CT then prevents in long term bacteria adhesion, after the complete release of the peptide. A preliminary moderate antibacterial action has been registered with respect to *S. Aureus*. The effectiveness of the antimicrobial activity of nisin-coated CT was significantly higher than the one registered on the untreated titanium, where only the antifouling effect was observed: no decrease of CFU number was observed compared to the nisin-free control. The higher amount of nisin at CT surface, as well as the higher release, were able to promote a proper antimicrobial response. A synergistic effect of the nanotexture of the substrate, preventing bacteria adhesion, and active antibacterial action of nisin can be supposed to be effective in limiting biofilm formation. An optimization of the adsorption protocol and further biological characterization will be performed to investigate the potentiality of this optimized nisin-coated surface.

## CRediT authorship contribution statement

**Virginia Alessandra Gobbo:** Investigation, Writing – original draft, Writing – review & editing, Visualization. **Mari Lallukka:** Investigation, Writing – review & editing. **Francesca Gamna:** Investigation, Writing – review & editing. **Mirko Prato:** Investigation, Writing – review & editing. **Alessandra Vitale:** Investigation, Writing – review & editing. **Sara Ferraris:** Conceptualization, Methodology, Writing – review & editing. **Ziba Najmi:** Investigation, Writing – review & editing. **Andrea Cochis:** Methodology, Resources, Writing – review & editing, Visualization. **Lia Rimondini:** Methodology, Resources, Writing – review & editing, Project administration, Funding acquisition. **Jonathan Massera:** Resources, Writing – review & editing, Project administration, Funding acquisition. **Silvia Spriano:** Conceptualization, Methodology, Resources, Writing – original draft, Writing – review & editing, Visualization, Supervision, Project administration, Funding acquisition.

## Declaration of Competing Interest

The authors declare the following financial interests/personal relationships which may be considered as potential competing interests: [Virginia Alessandra Gobbo reports was provided by Horizon 2020. Silvia Spriano has patent Multifunctional titanium surfaces for bone integration licensed to 2214732.].

## Data availability

No data was used for the research described in the article.

*Acknowledgments*

This study was funded by the European Union's Horizon 2020 Research and Innovation Program under Marie Skłodowska-Curie grant agreement No 860462-Project PREMUROSA to V. A. Gobbo and M. Lallukka.

Centro Interdipartimentale Polito BioMEDLab is acknowledged for supporting the measurements by the laser confocal microscope.

## Appendix A. Supplementary material

Supplementary data to this article can be found online at https://doi.org/10.1016/j.apsusc.2023.156820.

## References

[1] R.P. Verma, Titanium based biomaterial for bone implants: A mini review, Mater. Today:. Proc. 26 (2020) 3148–3151, https://doi.org/10.1016/j.matpr.2020.02.649.
[2] J. Zheng, L. Chen, D. Chen, C. Shao, M. Yi, B. Zhang, Effects of pore size and porosity of surface-modified porous titanium implants on bone tissue ingrowth, Trans. Nonferrous Met. Soc. Chin. 29 (2019) 2534–2545, https://doi.org/10.1016/S1003-6326(19)65161-7.
[3] H. Singh, R. Kumar, C. Prakash, S. Singh, HA-based coating by plasma spray techniques on titanium alloy for orthopedic applications, Mater. Today:. Proc. 50 (2022) 612–628, https://doi.org/10.1016/j.matpr.2021.03.165.
[4] T. Mokabber, L.Q. Lu, P. van Rijn, A.I. Vakis, Y.T. Pei, Crystal growth mechanism of calcium phosphate coatings on titanium by electrochemical deposition, Surf. Coat. Technol. 334 (2018) 526–535, https://doi.org/10.1016/j.surfcoat.2017.12.011.
[5] N.F. Mohammad, R.N. Ahmad, N.L.M. Rosli, M.S.A. Manan, M. Marzuki, A. Wahi, Sol gel deposited hydroxyapatite-based coating technique on porous titanium niobium for biomedical applications: A mini review, Mater. Today:. Proc. 41 (2021) 127–135, https://doi.org/10.1016/j.matpr.2020.11.1023.
[6] S. Ferraris, A. Venturello, M. Miola, A. Cochis, L. Rimondini, S. Spriano, Antibacterial and bioactive nanostructured titanium surfaces for bone integration, Appl. Surf. Sci. 311 (2014) 279–291, https://doi.org/10.1016/j.apsusc.2014.05.056.
[7] G. Wang, H. Fu, Y. Zhao, K. Zhou, S. Zhu, Bone integration properties of antibacterial biomimetic porous titanium implants, Transactions of Nonferrous Metals Society of China. 27 (2017) 2007–2014, https://doi.org/10.1016/S1003-6326(17)60225-5.
[8] M. Tarnowski, T. Borowski, S. Skrzypek, K. Kulikowski, T. Wierzchoń, Shaping the structure and properties of titanium and Ti6Al7Nb titanium alloy in low-temperature plasma nitriding processes, J. Alloy. Compd. 864 (2021), 158896, https://doi.org/10.1016/j.jallcom.2021.158896.
[9] Y. Yang, J. Liu, M. Chen, P. Gao, Y. Gong, R. Chen, Y. Tang, W. Yang, K. Cai, Photolithographic-based stamp technique for improving the biocompatibility of antibacterial titanium implant by dynamic clearance of antibacterial agents, Chem. Eng. J. 421 (2021), 129756, https://doi.org/10.1016/j.cej.2021.129756.
[10] S. Ferraris, S. Spriano, Antibacterial titanium surfaces for medical implants, Mater. Sci. Eng. C 61 (2016) 965–978, https://doi.org/10.1016/j.msec.2015.12.062.
[11] https://www.who.int/news-room/fact-sheets/detail/antimicrobial-resistance - visited on 16.09.2021.
[12] A. Asenjo, J. Oteo-Iglesias, J.-I. Alós, What's new in mechanisms of antibiotic resistance in bacteria of clinical origin? Enfermedades Infecciosas y Microbiologia Clinica (English Ed.) 39 (2021) 291–299, https://doi.org/10.1016/j.eimce.2020.02.017.
[13] E. Zhang, X. Zhao, J. Hu, R. Wang, S. Fu, G. Qin, Antibacterial metals and alloys for potential biomedical implants, Bioact. Mater. 6 (2021) 2569–2612, https://doi.org/10.1016/j.bioactmat.2021.01.030.

[14] J.J.T.M. Swartjes, P.K. Sharma, T.G. van Kooten, H.C. van der Mei, M. Mahmoudi, H.J. Busscher, E.T.J. Rochford, Current Developments in Antimicrobial Surface Coatings for Biomedical Applications, Curr. Med. Chem. 22 (2015) 2116–2129.

[15] R. Jiang, L. Hao, L. Song, L. Tian, Y. Fan, J. Zhao, C. Liu, W. Ming, L. Ren, Lotus-leaf-inspired hierarchical structured surface with non-fouling and mechanical bactericidal performances, Chem. Eng. J. 398 (2020), 125609, https://doi.org/10.1016/j.cej.2020.125609.

[16] J. Xu, X. Wu, Z. Lian, H. Yu, Y. Hou, X. Nie, Micro-nano manufacturing of Ti6Al4V antibacterial surface, Colloids Surf A Physicochem Eng Asp 625 (2021), 126929, https://doi.org/10.1016/j.colsurfa.2021.126929.

[17] S. Ferraris, A. Cochis, M. Cazzola, M. Tortello, A. Scalia, S. Spriano, L. Rimondini, Cytocompatible and Anti-bacterial Adhesion Nanotextured Titanium Oxide Layer on Titanium Surfaces for Dental and Orthopedic Implants, Front. Bioeng. Biotechnol. 7 (2019) 103, https://doi.org/10.3389/fbioe.2019.00103.

[18] S. Ferraris, F. Warchomicka, C. Ramskogler, M. Tortello, A. Cochis, A. Scalia, G. G. di Confiengo, J. Keckes, L. Rimondini, S. Spriano, Surface structuring by Electron Beam for improved soft tissues adhesion and reduced bacterial contamination on Ti-grade 2, J. Mater. Process. Technol. 266 (2019) 518–529, https://doi.org/10.1016/j.jmatprotec.2018.11.026.

[19] J. Małaczewska, E. Kaczorek-Łukowska, Nisin—A lantibiotic with immunomodulatory properties: A review, Peptides 137 (2021), 170479, https://doi.org/10.1016/j.peptides.2020.170479.

[20] J.M. Shin, J.W. Gwak, P. Kamarajan, J.C. Fenno, A.H. Rickard, Y.L. Kapila, Biomedical applications of nisin, J. Appl. Microbiol. 120 (2016) 1449–1465, https://doi.org/10.1111/jam.13033.

[21] K. Kuwano, N. Tanaka, T. Shimizu, K. Nagatoshi, S. Nou, K. Sonomoto, Dual antibacterial mechanisms of nisin Z against Gram-positive and Gram-negative bacteria, Int. J. Antimicrob. Agents 26 (2005) 396–402, https://doi.org/10.1016/j.ijantimicag.2005.08.010.

[22] E. Breukink, B. de Kruijff, The lantibiotic nisin, a special case or not?, Biochimica et Biophysica Acta (BBA) -, Biomembranes 1462 (1999) 223–234, https://doi.org/10.1016/S0005-2736(99)00208-4.

[23] Z. Tan, J. Luo, F. Liu, Q. Zhang, S. Jia, Effects of pH, Temperature, Storage Time, and Protective Agents on Nisin Antibacterial Stability, in: T.-.-C. Zhang, M. Nakajima (Eds.), Advances in Applied Biotechnology, Springer, Berlin Heidelberg, Berlin, Heidelberg, 2015, pp. 305–312, https://doi.org/10.1007/978-3-662-46318-5_33.

[24] H.M. Espejo, D.F. Bahr, Application of oxidized metallic surfaces as a medium to store biochemical agents with antimicrobial properties, Surf. Coat. Technol. 372 (2019) 312–318, https://doi.org/10.1016/j.surfcoat.2019.05.059.

[25] T. Lou, X. Bai, X. He, C. Yuan, Antifouling performance analysis of peptide-modified glass microstructural surfaces, Appl. Surf. Sci. 541 (2021), 148384, https://doi.org/10.1016/j.apsusc.2020.148384.

[26] A. Héquet, V. Humblot, J.-M. Berjeaud, C.-M. Pradier, Optimized grafting of antimicrobial peptides on stainless steel surface and biofilm resistance tests, Colloids Surf. B Biointerfaces 84 (2011) 301–309, https://doi.org/10.1016/j.colsurfb.2011.01.012.

[27] J. Aveyard, J.W. Bradley, K. McKay, F. McBride, D. Donaghy, R. Raval, R.A. D'Sa, Linker-free covalent immobilization of nisin using atmospheric pressure plasma induced grafting, Journal of Material Chemistry B. 5 (2017) 2500–2510, https://doi.org/10.1039/C7TB00113D.

[28] M. Lallukka, F. Gamna, V.A. Gobbo, M. Prato, Z. Najmi, A. Cochis, L. Rimondini, S. Ferraris, S. Spriano, Surface Functionalization of Ti6Al4V-ELI Alloy with Antimicrobial Peptide Nisin, Nanomaterials 12 (2022), https://doi.org/10.3390/nano12234332.

[29] Z. Zhao, J. Chen, H. Tan, X. Lin, W. Huang, Evolution of plastic deformation and its effect on mechanical properties of laser additive repaired Ti64ELI titanium alloy, Opt. Laser Technol. 92 (2017) 36–43, https://doi.org/10.1016/j.optlastec.2016.12.038.

[30] S.M. Spriano, E. Vernè, S. Ferraris, Multifunctional titanium surfaces for bone integration, European Patent 2214732 (2007).

[31] G. Riccucci, M. Cazzola, S. Ferraris, V.A. Gobbo, M. Guaita, S. Spriano, Surface functionalization of Ti6Al4V with an extract of polyphenols from red grape pomace, Mater. Des. 206 (2021), 109776, https://doi.org/10.1016/j.matdes.2021.109776.

[32] M. Roy, A. Pompella, J. Kubacki, J. Szade, R.A. Roy, W. Hedzelek, Photofunctionalization of Titanium: An Alternative Explanation of Its Chemical-Physical Mechanism, PLoS One 11 (2016) 1–11, https://doi.org/10.1371/journal.pone.0157481.

[33] H.M. Espejo, S. Díaz-Amaya, L.A. Stanciu, D.F. Bahr, Nisin infusion into surface cracks in oxide coatings to create an antibacterial metallic surface, Mater. Sci. Eng. C 105 (2019), 110034, https://doi.org/10.1016/j.msec.2019.110034.

[34] M. Koike, H. Fujii, The corrosion resistance of pure titanium in organic acids, Biomaterials 22 (2001) 2931–2936, https://doi.org/10.1016/S0142-9612(01)00040-0.

[35] N. Schiff, B. Grosgogeat, M. Lissac, F. Dalard, Influence of fluoride content and pH on the corrosion resistance of titanium and its alloys, Biomaterials 23 (2002) 1995–2002, https://doi.org/10.1016/S0142-9612(01)00328-3.

[36] S. Wu, Polymer interface and adhesion, 1st ed., Routledge, 1982. https://doi.org/10.1201/9780203742860.

[37] N. Fairley, V. Fernandez, M. Richard-Plouet, C. Guillot-Deudon, J. Walton, E. Smith, D. Flahaut, M. Greiner, M. Biesinger, S. Tougaard, D. Morgan, J. Baltrusaitis, Systematic and collaborative approach to problem solving using X-ray photoelectron spectroscopy, Applied Surface Science Advances. 5 (2021) 100112. https://doi.org/10.1016/j.apsadv.2021.100112.

[38] Y. Liu, J.L. Gilbert, The effect of simulated inflammatory conditions and Fenton chemistry on the electrochemistry of CoCrMo alloy, Journal of Biomedical Materials Research Part B: Applied, Biomaterials 106 (2018) 209–220, https://doi.org/10.1002/jbm.b.33830.

[39] L.R. Rivera, A. Cochis, S. Biser, E. Canciani, S. Ferraris, L. Rimondini, A. R. Boccaccini, Antibacterial, pro-angiogenic and pro-osteointegrative zein-bioactive glass/copper based coatings for implantable stainless steel aimed at bone healing, Bioact. Mater. 6 (2021) 1479–1490, https://doi.org/10.1016/j.bioactmat.2020.11.001.

[40] A. Cochis, J. Barberi, S. Ferraris, M. Miola, L. Rimondini, E. Vernè, S. Yamaguchi, S. Spriano, Competitive surface colonizaion of antibacterial and bioactive materials doped with strontium and/or silver ions, Nanomaterials 10 (2020) 120, https://doi.org/10.3390/nano10010120.

[41] J.J. Harrison, C.A. Stremick, R.J. Turner, N.D. Allan, M.E. Olson, H. Ceri, Microtiter susceptibility testing of microbes growing on peg lids: a miniaturized biofilm model for high-throughput screening, Nat. Protoc. 5 (2010) 1236–1254, https://doi.org/10.1038/nprot.2010.71.

[42] A.P. Tchinda, G. Pierson, R. Kouitat-Njiwa, P. Bravetti, The surface conditions and composition of titanium alloys in implantology: A comparative study of dental implants of different brands, Materials. 15 (2022) 1018, https://doi.org/10.3390/ma15031018.

[43] R. Zahran, J.I. Rosales Leal, M.A. Rodríguez Valverde, M.A. Cabrerizo Vilchez, Effect of hydrofluoric acid etching time on titanium topography, chemistry, wettability, and cell adhesion, PLos ONE. 11 (n.d.) e0165296. https://doi.org/10.1371/journal.pone.0165296.

[44] R. Pandit, M. Rai, C.A. Santos, Enhanced antimicrobial activity of the food-protecting nisin peptide by bioconjugation with silver nanoparticles, Environ. Chem. Lett. 15 (2017) 443–452, https://doi.org/10.1007/s10311-017-0626-2.

[45] R. Chang, H. Lu, M. Li, S. Zhang, L. Xiong, Q. Sun, Preparation of extra-small nisin nanoparticles for enhanced antibacterial activity after autoclave treatment, Food Chem. 245 (2018) 756–760, https://doi.org/10.1016/j.foodchem.2017.11.116.

[46] J. Qian, Y. Chen, Q. Wang, X. Zhao, H. Yang, F. Gong, H. Guo, Preparation and antimicrobial activity of pectin-chitosan embedding nisin microcapsules, Eur. Polym. J. 157 (2021), 110676, https://doi.org/10.1016/j.eurpolymj.2021.110676.

[47] H. Fael, A.L. Demirel, Nisin/polyanion layer-by-layer films exhibiting different mechanisms in antimicrobial efficacy, RSC Adv. 10 (2020) 10329–10337, https://doi.org/10.1039/C9RA10135G.

[48] H.S. Rollema, O.P. Kuipers, P. Both, W.M. de Vos, R.J. Siezen, Improvement of solubility and stability of the antimicrobial peptide nisin by protein engineering, Appl. Environ. Microbiol. 61 (1995) 2873–2878, https://doi.org/10.1128/aem.61.8.2873-2878.1995.

[49] M. Kulkarni, Y. Patil-Sen, I. Junkar, C.V. Kulkarni, M. Lorenzetti, A. Iglič, Wettability studies of topologically distinct titanium surfaces, Colloids Surf. B Biointerfaces 129 (2015) 47–53, https://doi.org/10.1016/j.colsurfb.2015.03.024.

[50] S. Ferraris, S. Spriano, M. Miola, E. Bertone, V. Allizond, A.M. Cuffini, G. Banche, Surface modification of titanium surfaces through a modified oxide layer and embedded silver nanoparticles: Effect of reducing/stabilizing agents on precipitation and properties of the nanoparticles, Surf. Coat. Technol. 344 (2018) 177–189, https://doi.org/10.1016/j.surfcoat.2018.03.020.

[51] Z. Yu, L. Ma, S. Ye, G. Li, M. Zhang, Construction of an environmentally friendly octenylsuccinic anhydride modified pH-sensitive chitosan nanoparticle drug delivery system to alleviate inflammation and oxidative stress, Carbohydr. Polym. 236 (2020), 115972, https://doi.org/10.1016/j.carbpol.2020.115972.

[52] J.E. Wampler, D.E. Stewart, S.L. Gallion, Molecular Dynamics Simulations of Proteins and Protein-Protein Complexes, in: D.P. Landau, K.K. Mon, H.-.-B. Schüttler (Eds.), Computer Simulation Studies in Condensed Matter Physics II, Springer, Berlin Heidelberg, Berlin, Heidelberg, 1990, pp. 68–84.

[53] M. Textor, C. Sittig, V. Frauchiger, S. Tosatti, D.M. Brunette, Properties and Biological Significance of Natural Oxide Films on Titanium and Its Alloys, in: Titanium in Medicine: Material Science, Surface Science, Engineering, Biological Responses and Medical Applications, Springer, Berlin Heidelberg, Berlin, Heidelberg, 2001, pp. 171–230, https://doi.org/10.1007/978-3-642-56486-4_7.

[54] M. Morra, C. Cassinelli, G. Buzzone, A. Carpi, G. Di Santi, R. Giardino, M. Fini, Surface chemistry effect of topographical modification of titanium dental implant surfaces: 1, Surf. Anal. Int. J. Oral Maxillofacial Implants. 18 (2003) 40–45.

[55] S. Ferraris, M. Prato, C. Vineis, A. Varesano, G.G. di Confiengo, S. Spriano, Coupling of keratin with titanium: A physico-chemical characterization of functionalized or coated surfaces, Surf. Coat. Technol. 397 (2020), 126057, https://doi.org/10.1016/j.surfcoat.2020.126057.

[56] O. Cavalleri, G. Gonella, S. Terreni, M. Vignolo, L. Floreano, A. Morgante, M. Canepa, R. Rolandi, High resolution X-ray photoelectron spectroscopy of l-cysteine self-assembled films, PCCP 6 (2004) 4042–4046, https://doi.org/10.1039/B405516K.

[57] NIST X-ray Photoelectron Spectroscopy Database, Version 4.1 (National Institute of Standards and Technology, Gaithersburg, 2012). http://srdata.nist.gov/xps/.

[58] J.O. Hollinger, An Introduction to Biomaterials, CRC Press, Taylor & Francis Group, Boca Raton, FL, 2012.

[59] F. Gamna, A. Cochis, A.C. Scalia, A. Vitale, S. Ferraris, L. Rimondini, S. Spriano, The use of vitamin E as an anti-adhesive coating for cells and bacteria for temporary bone implants, Surf. Coat. Technol. 444 (2022), 128694, https://doi.org/10.1016/j.surfcoat.2022.128694.

[60] S. Spriano, V.S. Chandra, A. Cochis, F. Uberti, L. Rimondini, E. Bertone, A. Vitale, C. Scolaro, M. Ferrari, F. Cirisano, G.G. di Confiengo, S. Ferraris, How do wettability, zeta potential and hydroxylation degree affect the biological response of biomaterials? Mater. Sci. Eng. C 74 (2017) 542–555, https://doi.org/10.1016/j.msec.2016.12.107.

[61] M. Rahnamaeian, Antimicrobial peptides, Plant Signal. Behav. 6 (2011) 1325–1332, https://doi.org/10.4161/psb.6.9.16319.
[62] Z. Najmi, A. Kumar, A.C. Scalia, A. Cochis, B. Obradovic, F.A. Grassi, M. Leigheb, M. Lamghari, I. Loinaz, R. Gracia, L. Rimondini, Evaluation of Nisin and LL-37 Antimicrobial Peptides as Tool to Preserve Articular Cartilage Healing in a Septic Environment, Front. Bioeng. Biotechnol. 8 (2020) 561, https://doi.org/10.3389/fbioe.2020.00561.
[63] J. Koziel, J. Potempa, Protease-armed bacteria in the skin, Cell and Tissue, Research 351 (2013) 325–337, https://doi.org/10.1007/s00441-012-1355-2.
[64] A. Shivaee, S. Rajabi, H.E. Farahani, A.A.I. Fooladi, Effect of sub-lethal doses of nisin on Staphylococcus aureus toxin production and biofilm formation, Toxicon 197 (2021) 1–5, https://doi.org/10.1016/j.toxicon.2021.03.018.
[65] F.P. da Silva, K.M. Fernandes, L.L. de Freitas, R. de S. Cascardo, R.C. Bernardes, L.L. de Oliveira, G.F. Martins, M.C.D. Vanetti, Effects of sub-lethal doses of nisin on the virulence of Salmonella enterica in Galleria mellonella larvae, Res. Microbiol. 172 (2021) 103836. https://doi.org/10.1016/j.resmic.2021.103836.
[66] R. Sorrentino, A. Cochis, B. Azzimonti, C. Caravaca, J. Chevalier, M. Kuntz, A. A. Porporati, R.M. Streicher, L. Rimondini, Reduced bacterial adhesion on ceramics used for arthroplasty applications, J. Eur. Ceram. Soc. 38 (2018) 963–970, https://doi.org/10.1016/j.jeurceramsoc.2017.10.008.
[67] L.D. Blackman, M.K. Fros, N.G. Welch, T.R. Gengenbach, Y. Qu, P. Pasic, P. A. Gunatillake, H. Thissen, P. Cass, K.E.S. Locock, Dual Action Antimicrobial Surfaces: Alternating Photopatterns Maintain Contact-Killing Properties with Reduced Biofilm Formation, Macromol. Mater. Eng. 305 (2020) 2070026, https://doi.org/10.1002/mame.202000371.
[68] J. Kim, K. Kim, Y.-S. Choi, H. Kang, D.M. Kim, J.-C. Lee, Polysulfone based ultrafiltration membranes with dopamine and nisin moieties showing antifouling and antimicrobial properties, Sep. Purif. Technol. 202 (2018) 9–20, https://doi.org/10.1016/j.seppur.2018.03.033.
[69] C. Roupie, B. Labat, S. Morin-Grognet, P. Thébault, G. Ladam, Nisin-based antibacterial and antiadhesive layer-by-layer coatings, Colloids and Surfaces, B, Biointerfaces. 208 (2021), 112121, https://doi.org/10.1016/j.colsurfb.2021.112121.